

Neutrino-induced meson productions

Satoshi X. NAKAMURA

Department of Physics, Osaka University, Toyonaka, Osaka 560-0043, Japan

E-mail: nakamura@kern.phys.sci.osaka-u.ac.jp

(Received October 1, 2015)

We develop a dynamical coupled-channels (DCC) model for neutrino-nucleon reactions in the resonance region, by extending the DCC model that we have previously developed through an analysis of $\pi N, \gamma N \rightarrow \pi N, \eta N, K\Lambda, K\Sigma$ reaction data for $W \leq 2.1$ GeV. We analyze electron-induced reaction data for both proton and neutron targets to determine the vector current form factors up to $Q^2 \leq 3.0$ (GeV/c)². Axial-current matrix elements are derived in accordance with the Partially Conserved Axial Current (PCAC) relation to the πN interactions of the DCC model. As a result, we can uniquely determine the interference pattern between resonant and non-resonant amplitudes. Our calculated cross sections for neutrino-induced single-pion productions are compared with available data, and are found to be in reasonable agreement with the data. We also calculate the double-pion production cross sections in the resonance region, for the first time, with relevant resonance contributions and channel couplings. The result is compared with the double-pion production data. For a future development of a neutrino-nucleus reaction model and/or a neutrino event generator for analyses of neutrino experiments, the DCC model presented here can give a useful input.

KEYWORDS: Neutrino-nucleus interactions, Meson production, Meson-baryon interactions, neutrino oscillation

1. Introduction

More improved understanding of neutrino-nucleus reactions is a critical issue for addressing the leptonic CP violation and the neutrino mass hierarchy with forthcoming neutrino oscillation experiments. The neutrino oscillation experiments utilize neutrinos in a wide energy range, and therefore the relevant neutrino-nucleus reactions have various microscopic reaction mechanisms depending on the kinematics. For a relatively low-energy neutrino ($E_\nu \lesssim 1$ GeV), the dominant reaction mechanisms are the quasi-elastic knockout of a nucleon, and quasi-free excitation of the $\Delta(1232)$ resonance followed by a decay into a πN final state. For a higher-energy neutrino ($2 \lesssim E_\nu \lesssim 4$ GeV), a large portion of data are from higher resonance excitations and deep inelastic scattering (DIS). In order to understand the neutrino-nucleus reactions of these different characteristics, obviously, it is important to combine different expertise. For example, nuclear theorists and neutrino experimentalists recently organized a collaboration at the J-PARC branch of the KEK theory center [1,2] to tackle this challenging problem.

In this work, we focus on studying the neutrino reactions in the resonance region where the total hadronic energy W extends, $m_N + m_\pi < W \lesssim 2$ GeV; m_N (m_π) is the nucleon (pion) mass. Furthermore we will be concerned with the neutrino reaction on a single nucleon. In the resonance region, particularly between the $\Delta(1232)$ and DIS regions, we are still in the stage of developing a single nucleon model that is a basic ingredient to construct a neutrino-nucleus reaction model. Several theoretical models have been developed for neutrino-nucleon reactions in the resonance region; particularly the $\Delta(1232)$ region has been extensively studied because of its importance. However, there still remain conceptual and/or practical problems in the existing models as follows: First, we point out that reactions in the resonance region are multi-channel processes in nature. However, no existing model takes account of the multi-channel couplings required by the unitarity. Second, the neutrino-induced

double pion productions over the entire resonance region have not been seriously studied previously, even though their production rates are expected to be comparable or even more important than those for the single-pion productions around and beyond the second resonance region. Third, interference between resonant and non-resonant amplitudes are not well under control for the axial-current in most of the previous models.

Our goal here is to develop a neutrino-nucleon reaction model in the resonance region by overcoming the problems discussed above. In order to do so, the best available option would be to work with a coupled-channels model. In the last few years, we have developed a dynamical coupled-channels (DCC) model to analyze $\pi N, \gamma N \rightarrow \pi N, \eta N, K\Lambda, K\Sigma$ reaction data for a study of the baryon spectroscopy [3]. In there, we have shown that the model is successful in giving a reasonable fit to a large amount ($\sim 23,000$ data points) of the data. The model also has been shown to give a reasonable prediction for the pion-induced double pion productions [4]. Thus the DCC model seems a promising starting point for developing a neutrino-reaction model in the resonance region. At $Q^2 = 0$, we already have made an extension of the DCC model to the neutrino sector by invoking the PCAC (Partially Conserved Axial Current) hypothesis [5]. At this particular kinematics, the cross section is given by the divergence of the axial-current amplitude that is related to the πN amplitude through the PCAC relation. However, for describing the neutrino reactions in the whole kinematical region ($Q^2 \neq 0$), a dynamical model for the vector- and axial-currents is needed.

Practically, we need to do the following tasks for extending the DCC model to cover the neutrino reactions. Regarding the vector current, we already have fixed the amplitude for the proton target at $Q^2=0$ in our previous analysis [3]. The remaining task is to determine the Q^2 -dependence of the vector couplings, i.e., form factors. This can be done by analyzing data for the single pion electroproduction and inclusive electron scattering. A similar analysis also needs to be done with the neutron target model. By combining the vector current amplitudes for the proton and neutron targets, we can do the isospin separation of the vector current. This is a necessary step before calculating neutrino processes. As for the axial-current matrix elements at $Q^2=0$, we derive them so that the consistency, required by the PCAC relation, with the DCC πN interaction model is maintained. As a result of this derivation, the interference pattern between the resonant and non-resonant amplitudes are uniquely fixed within our model; this is an advantage of our approach. For the Q^2 -dependence of the axial-current matrix elements, we still inevitably need to employ a simple ansatz due to the lack of experimental information. This is a limitation shared by all the existing neutrino-reaction models in the resonance region.

With the vector- and axial-currents as described above, we calculate cross sections for the neutrino-induced meson productions in the resonance region. We compare our numerical results with available data for single-pion and double-pion productions. Particularly, comparison with the double-pion production data is made for the first time with the relevant resonance contributions and coupled-channels effects taken into account. For a fuller presentation of this work, we refer the readers to Ref. [6].

2. Formalism

The weak interaction Lagrangian for charged-current (CC) processes is given by

$$\mathcal{L}^{\text{CC}} = \frac{G_F V_{ud}}{\sqrt{2}} \int d^3x [J_\mu^{\text{CC}}(x) l^{\text{CC}\mu}(x) + \text{h.c.}], \quad (1)$$

where G_F is the Fermi coupling constant and V_{ud} is the CKM matrix element. The leptonic current is denoted by l_μ^{CC} , while the hadronic current is

$$J_\mu^{\text{CC}}(x) = V_\mu^+(x) - A_\mu^+(x), \quad (2)$$

where V_μ^+ and A_μ^+ are the vector and axial currents. The superscript + denotes the isospin raising operator.

2.1 Matrix elements of non-resonant currents

As in Eqs. (2), the current consists of the vector and axial currents. Matrix elements of the non-resonant vector current at $Q^2 = 0$ have been fixed through the previous analysis of photon-induced meson-production data [3]. We also need to fix the Q^2 -dependence of the matrix elements to study electron- and neutrino-induced reactions. Regarding the axial current, we take advantage of the fact that most of our $\pi N \rightarrow MB$ (MB : a meson-baryon state) potentials are derived from a chiral Lagrangian. Thus, we basically follow the way how the axial current is introduced in the chiral Lagrangian: an external axial current (a_{ext}^μ) enters into the chiral Lagrangian in combination with the pion field as $\partial^\mu \pi + f_\pi a_{\text{ext}}^\mu$ where f_π is the pion decay constant. Then the tree-level non-resonant axial-current matrix elements are derived from the chiral Lagrangian. By construction, $A_{\text{NP,tree}}^{i\mu}$ (i : isovector component) and the meson-baryon potential v satisfy the PCAC relation at $Q^2 = -m_\pi^2$: $\langle MB|q \cdot A_{\text{NP,tree}}^i|N \rangle = i f_\pi \langle MB|v|\pi^i N \rangle$. The Q^2 -dependence of the axial-coupling to the nucleon is fairly well-known from data analyses of quasi-elastic neutrino scattering and single pion electroproduction near threshold. We employ the conventional dipole form factor, $F_A(Q^2) = 1/(1 + Q^2/M_A^2)$, and take a numerical value for the axial mass, $M_A = 1.02$ GeV, from Ref. [7].

2.2 Matrix elements of N^* -excitation currents

The hadronic vector current contributes to the neutrino-induced reactions in the finite Q^2 region. In Ref. [3], we have done a combined analysis of $\pi N, \gamma p \rightarrow \pi N, \eta N, K\Lambda, K\Sigma$ reaction data, and fixed matrix elements of the vector current at $Q^2 = 0$ for the proton target. What we need to do is to extend the matrix elements of the vector current of Ref. [3] to the finite Q^2 region for application to the neutrino reactions. This can be done by analyzing data for electron-induced reactions on the proton and the neutron. Then we separate the vector form factors for N^* of $I = 1/2$ (I : isospin) into isovector and isoscalar parts. Regarding N^* of $I = 3/2$ for which only the isovector current contributes, we can determine the vector form factors by analyzing the proton-target data.

Because of rather scarce neutrino reaction data, it is difficult to determine N - N^* transition matrix elements induced by the axial-current. This is in sharp contrast with the situation for the vector form factors that are well determined by a large amount of electromagnetic reaction data. Thus, we need to take a different path to fix the axial form factors. The conventional practice is to write down a N - N^* transition matrix element induced by the axial-current in a general form with three or four form factors. Then the PCAC relation, $\langle N^*|q \cdot A_{\text{NP}}^i|N \rangle = i f_\pi \langle N^*|\Gamma|\pi^i N \rangle$, is invoked to relate the presumably most important axial form factor at $Q^2 = -m_\pi^2$ to the corresponding πNN^* coupling. The other form factors are ignored except for the pion pole term. We then assume $A_{\text{NP}}^{i\mu}(Q^2 = -m_\pi^2) \sim A_{\text{NP}}^{i\mu}(Q^2 = 0)$. In the present work, we consider the axial currents for bare N^* of the spin-parity $1/2^\pm, 3/2^\pm, 5/2^\pm$ and $7/2^\pm$, and determine their axial form factors at $Q^2 = 0$ using the above procedure. It is even more difficult to determine the Q^2 -dependence of the axial couplings to N - N^* transitions because of the limited amount of data. Thus we assume that the Q^2 -dependence of the axial form factors is the same as that used for the non-resonant axial-current amplitudes. It is worth emphasizing that a great advantage of our approach over the existing models is that relative phases between resonant and non-resonant amplitudes are made under control within the DCC model. This is possible in our approach by constructing the axial-current amplitudes and πN interactions consistently with the requirement of the PCAC relation.

3. Analysis of electron-induced reaction data

Here we analyze data for electron-induced reactions off the proton and neutron targets to determine the Q^2 dependence of the vector form factors. The data we analyze span the kinematical region of $W \leq 2$ GeV and $Q^2 \leq 3$ (GeV/c)² that is also shared by neutrino reactions for $E_\nu \leq 2$ GeV.

Among data for electron-proton reactions in the resonance region, those for the single pion elec-

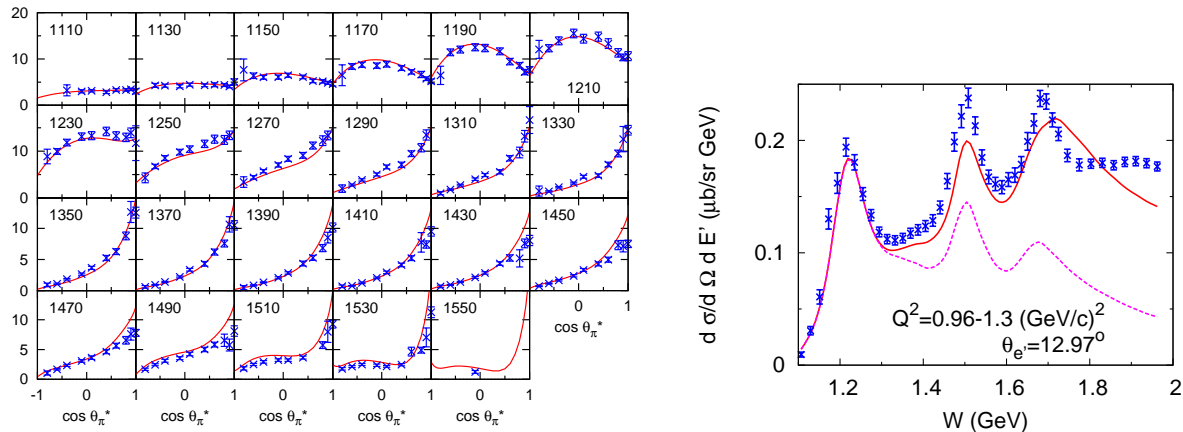


Fig. 1. (Color online) (Left) The virtual photon cross section $d\sigma_T/d\Omega_\pi^* + \epsilon d\sigma_L/d\Omega_\pi^*$ ($\mu\text{b/sr}$) at $Q^2=0.40$ (GeV/c)² for $p(e, e'\pi^+)n$ from the DCC model. The number in each panel indicates W (MeV). The data are from Ref. [9]. (Right) Comparison of DCC-based calculation with data for inclusive electron-proton scattering at $E_e=5.498$ GeV. The red solid curves are for inclusive cross sections while the magenta dashed-curves are for contributions from the πN final states. The range of Q^2 and the electron scattering angle ($\theta_{e'}$) are indicated in each panel. The data are from Ref. [10].

troproductions are the most abundant over a wide range of W and Q^2 . Therefore, these are the most useful to determine the Q^2 dependence of the p - N^* transition form factors. The cross sections for $p(e, e'\pi^0)p$ and $p(e, e'\pi^+)n$ have different sensitivities to resonances of different isospin state (1/2 or 3/2). The angular distribution of the pion is useful to disentangle the spin-parity of the resonances. Based on the one-photon exchange approximation, a standard formula of the angular distribution for the single pion electroproduction can be expressed in terms of virtual photon cross sections $d\sigma_\beta(Q^2, W, \cos\theta_\pi^*)/d\Omega_\pi^*$ ($\beta = T, L, LT, TT, LT'$).

The CLAS Collaboration has collected data for the single pion electroproduction off the proton in the kinematical region of our interest. Then they have extracted from the data the virtual photon cross sections. We fit these virtual photon cross sections to determine the Q^2 dependence of the p - N^* transition form factors. The single pion electroproduction data occupy a substantial portion of the relevant kinematical region of W and Q^2 . In some kinematical region, however, we still need more data to fix the vector form factors. In particular, data are missing for the $W \gtrsim 1.4$ GeV and low- Q^2 region, and the $W \gtrsim 1.7$ GeV and $Q^2 \lesssim 2$ (GeV/c)². In those kinematical region, we fit the inclusive structure functions from an empirical model due to Christy and Bosted [8].

We have fitted the data at several Q^2 values where the data are available. All the other parameters in the DCC model are fixed as those determined in Ref. [3]. We have successfully tested the DCC-based vector current model with the data covering the whole kinematical region relevant to neutrino reactions of $E_\nu \leq 2$ GeV. We present a selected result for the analysis of electron-proton reactions. We show a combination of the virtual photon cross sections, $d\sigma_T/d\Omega_\pi^* + \epsilon d\sigma_L/d\Omega_\pi^*$, at $Q^2=0.40$ (GeV/c)² for $p(e, e'\pi^+)n$ from the DCC model in Fig. 1 (left). In the same figure, the corresponding data are also shown for comparison. The DCC model fits the data for both π^0 and π^+ channels reasonably well. We also show in Fig. 1 (right) our DCC-based calculation of differential cross sections of the inclusive electron-proton scattering in comparison with data; the single pion electroproduction cross sections from the DCC model are also presented. In the figure, the range of Q^2 is indicated, and Q^2 monotonically decreases as W increases. The figures show a reasonable agreement between our calculation with the data, and also show the increasing importance of the multi-pion production processes above the $\Delta(1232)$ resonance region. As Q^2 increases, the DCC model starts to underestimate the inclusive cross section towards $W \sim 2$ GeV where the kinematical region is entering the DIS and

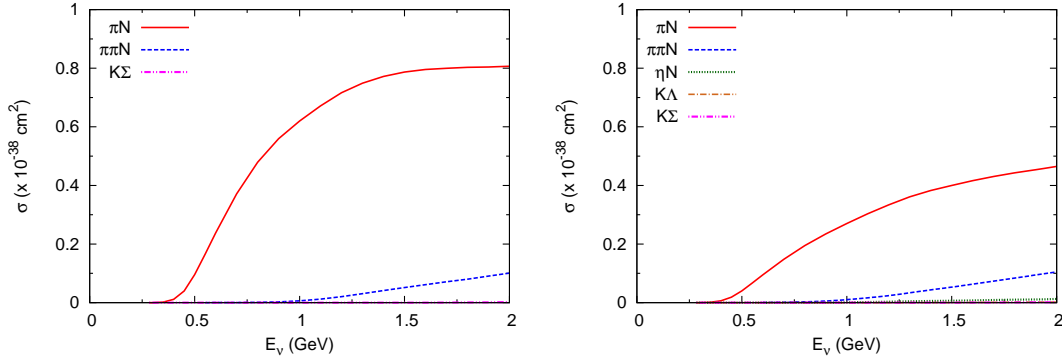


Fig. 2. (Color online) Total cross sections for the CC $\nu_\mu p$ (left) and $\nu_\mu n$ (right) reactions.

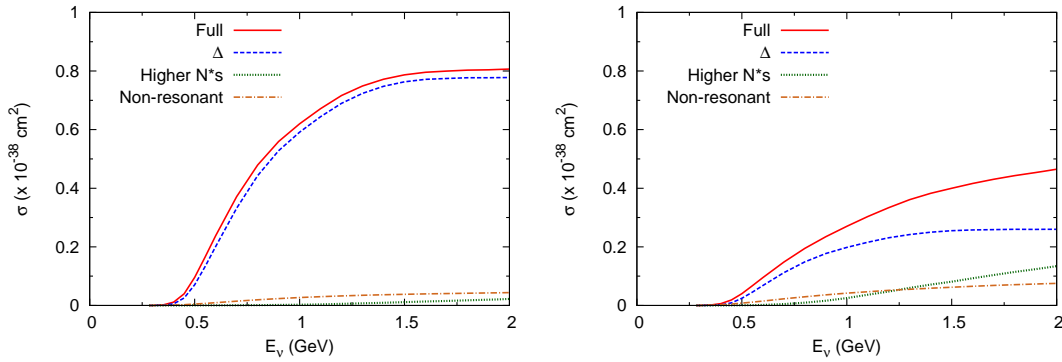


Fig. 3. (Color online) Various mechanisms contributing to $\nu_\mu p \rightarrow \mu^- \pi^+ p$ (left) and $\nu_\mu n \rightarrow \mu^- \pi N$ (right).

multi-meson production region.

Regarding the $\gamma n \rightarrow \pi N$ reactions, we analyze unpolarized differential cross sections data from πN threshold to $W = 2$ GeV, and determine the vector nN^* transition strengths at $Q^2=0$ for $I=1/2$ N^* states. In the finite Q^2 region, we use empirical inclusive structure functions from Ref. [11, 12] as data to determine the transition vector form factors. We successfully fitted the data by adjusting the vector form factors. See Ref. [6] for numerical results.

4. Results for neutrino reactions

We present cross sections for the $\nu_\mu N$ reactions. With the DCC model, we can predict contributions from all the final states included in our model. Also, the DCC model provides all possible differential cross sections for each channel. Here, we present total cross sections for the CC $\nu_\mu N$ reactions up to $E_\nu = 2$ GeV in Fig. 2. For the proton-target, the single pion production dominates in the considered energy region. For the neutron-target, the single pion production is still the largest, but double-pion production becomes relatively more important towards $E_\nu = 2$ GeV. The ηN and KY production cross sections are $O(10^{-1}-10^{-2})$ smaller.

Next we examine reaction mechanisms of the $\nu_\mu N$ scattering. In Fig. 3, we break down the single-pion production cross sections into several contributions each of which contains a set of certain mechanisms. For the proton-target process, the contribution from the $\Delta(1232)$ resonance dominates, while the higher N^* contribution is very small. The Δ contribution here is the neutrino cross section

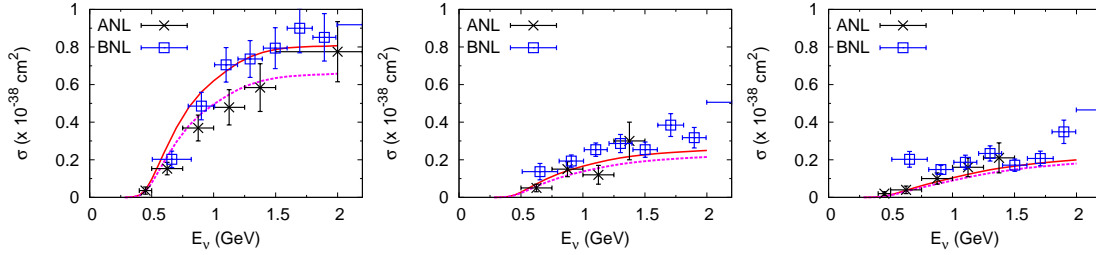


Fig. 4. (Color online) Comparison of the DCC-based calculation (red solid curves) with data for $\nu_\mu p \rightarrow \mu^- \pi^+ p$ (left), $\nu_\mu n \rightarrow \mu^- \pi^0 p$ (middle) and $\nu_\mu n \rightarrow \mu^- \pi^+ n$ (right). The DCC calculation with $0.8 \times g_{AN\Delta(1232)}^{\text{PCAC}}$ is also shown (magenta dashed curve). ANL (BNL) data are from Ref. [13] ([14]).

calculated with the P_{33} partial wave amplitude that contains the N^* -excitation mechanisms, while the higher N^* contribution is from the resonant amplitude including all partial waves other than P_{33} . The non-resonant cross sections calculated from the non-resonant amplitude is small for the proton-target process. In contrast, the situation is more complex in the neutron-target process where the Δ gives a smaller contribution and both $I = 1/2$ and $3/2$ resonances contribute. As can be seen in the right panel of Fig. 3, the Δ dominates for $E_\nu \lesssim 1$ GeV, and higher resonances and non-resonant mechanisms give comparable contributions towards $E_\nu \sim 2$ GeV. This shows an importance of including both resonant and non-resonant contributions with the interferences among them under control. Similarly, we can compare the contribution of resonant and non-resonant amplitudes for the two-pion production reaction. Because $\Delta(1232)$ mainly contributes below the $\pi\pi N$ production threshold and thus gives a small contribution here, the resonant and non-resonant contributions are more comparable. Still, we find that the resonance-excitations are the main mechanism for the double-pion production in the resonance region.

Next we compare the CC neutrino-induced single pion production cross sections from the DCC model with available data from Refs. [13, 14] in Fig. 4. The left panel shows the total cross sections for $\nu_\mu p \rightarrow \mu^- \pi^+ p$ for which $\Delta(1232)$ dominates as we have seen in Fig. 3. If the $\Delta(1232)$ -dominance persists in the neutron-target processes shown in the middle and right panels of Fig. 4, the isospin Clebsch-Gordan coefficients determine the relative strength as $\sigma(\nu_\mu n \rightarrow \mu^- \pi^0 p)/\sigma(\nu_\mu p \rightarrow \mu^- \pi^+ p) = 2/9 \sim 0.22$, and $\sigma(\nu_\mu n \rightarrow \mu^- \pi^+ n)/\sigma(\nu_\mu p \rightarrow \mu^- \pi^+ p) = 1/9 \sim 0.11$. The actual ratios from the DCC model are $\sigma(\nu_\mu n \rightarrow \mu^- \pi^0 p)/\sigma(\nu_\mu p \rightarrow \mu^- \pi^+ p) = 0.28, 0.27, 0.29$, and $\sigma(\nu_\mu n \rightarrow \mu^- \pi^+ n)/\sigma(\nu_\mu p \rightarrow \mu^- \pi^+ p) = 0.13, 0.17, 0.21$ at $E_\nu = 0.5, 1, 1.5$ GeV, respectively. The deviations from the naive isospin analysis are due to the non-resonant and higher-resonances contributions mostly in the neutron-target processes, as we have seen in Fig. 3. The two datasets from BNL and ANL for $\nu_\mu p \rightarrow \mu^- \pi^+ p$ shown in the left panel of Fig. 4 are not consistent as has been well known, and our result is closer to the BNL data [13]. For the other channels, our result is fairly consistent with both of the BNL and ANL data. It seems that the bare axial N - $\Delta(1232)$ coupling constants determined by the PCAC relation are too large to reproduce the ANL data. Because axial N - N^* coupling constants should be better determined by analyzing neutrino-reaction data, it is tempting to multiply the bare axial N - $\Delta(1232)$ coupling constants, $g_{AN\Delta(1232)}^{\text{PCAC}}$, by 0.8, so that the DCC model better fits the ANL data. The resulting cross sections are shown by the dashed curves in Fig. 4. We find that $\sigma(\nu_\mu p \rightarrow \mu^- \pi^+ p)$ is reduced due to the dominance of the $\Delta(1232)$ resonance in this channel, while $\sigma(\nu_\mu n \rightarrow \mu^- \pi N)$ is only slightly reduced. The original data of these two experimental data have been reanalyzed recently [15], and it was claimed that the discrepancy between the two datasets is resolved. The resulting cross sections are closer to the original ANL data. However, the number of data is still very limited, and a new measurement of neutrino cross sections on the hydrogen and deuterium is highly desirable. We also note that the data shown in Fig. 4 were taken from experiments using the deuterium target. Thus

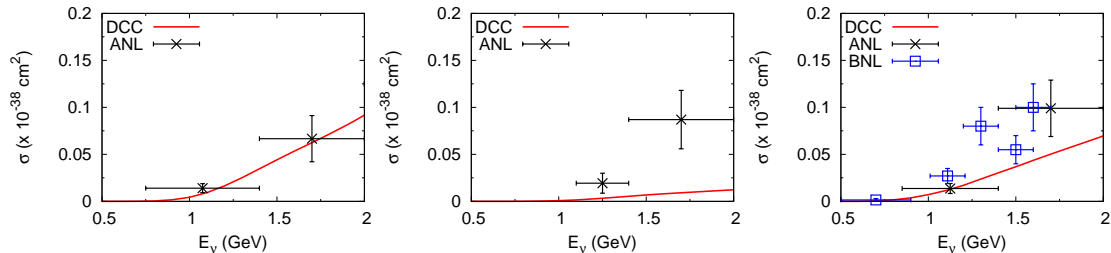


Fig. 5. (Color online) Comparison of the DCC-based calculation with data for $\nu_\mu p \rightarrow \mu^- \pi^+ \pi^0 p$ (left), $\nu_\mu p \rightarrow \mu^- \pi^+ \pi^+ n$ (middle) and $\nu_\mu n \rightarrow \mu^- \pi^+ \pi^- p$ (right). ANL (BNL) data are from Ref. [21] ([14]).

one should analyze the data considering the nuclear effects such as the initial two-nucleon correlation and the final state interactions. Recently, the authors of Ref. [16] have taken a first step towards such an analysis. They developed a model that consists of elementary amplitudes for neutrino-induced single pion production off the nucleon [17], pion-nucleon rescattering amplitudes, and the deuteron and final NN scattering wave functions. Although they did not analyze the ANL and BNL data with their model, they examined how much the cross sections at certain kinematics can be changed by considering the nuclear effects. They found that the cross sections can be reduced as much as 30% for $\nu_\mu d \rightarrow \mu^- \pi^+ pn$ due to the NN rescattering. Meanwhile, the cross sections for $\nu_\mu d \rightarrow \mu^- \pi^0 pp$ are hardly changed by the final state interaction. It will be important to analyze the ANL and BNL data with this kind of model to determine the axial nucleon current, particularly the axial $N\text{-}\Delta(1232)$ transition strength.

We finally compare our results for double-pion productions with existing data in Fig. 5. Although there exist a few theoretical works on the neutrino-induced double-pion production near threshold [18–20], our calculation for the first time takes account of relevant resonance contributions for this process. The DCC-based prediction is fairly consistent with the data in the order of the magnitude. Particularly, the cross sections for $\nu_\mu p \rightarrow \mu^- \pi^+ \pi^0 p$ from the DCC model are in agreement with data. However, the DCC prediction underestimates the $\nu_\mu p \rightarrow \mu^- \pi^+ \pi^+ n$ data. The rather small ratio of $\sigma(\nu_\mu p \rightarrow \mu^- \pi^+ \pi^+ n)/\sigma(\nu_\mu p \rightarrow \mu^- \pi^+ \pi^0 p) \sim 13\%$ at $E_\nu=2$ GeV from our calculation can be understood as follows. Within the present DCC-based calculation, $\pi\pi N$ final states are from decays of the πN and of the $\pi\Delta$, ρN , σN quasi two-body states. For a neutrino CC process on the proton for which hadronic states have $I = 3/2$, the πN , $\pi\Delta$, ρN channels can contribute. Within the current DCC model, we found that the $\pi\Delta$ channel gives a dominant contribution to the double pion productions. Then, retaining only the $\pi\Delta$ contribution, the ratio is given by the isospin Clebsch-Gordan coefficients as, $\sigma(\nu_\mu p \rightarrow \mu^- \pi^+ \pi^+ n)/\sigma(\nu_\mu p \rightarrow \mu^- \pi^+ \pi^0 p) = 2/13 \sim 15\%$, in good agreement with the ratio from the full calculation. With a very limited dataset, we do not further pursue the origin of the difference between our calculation and the data. If the double-pion data are further confirmed, then the model needs to incorporate some other mechanisms and/or adjust model parameters of the DCC model to explain the data.

5. Summary

In this work, we have developed a dynamical coupled-channels (DCC) model for neutrino-nucleon reactions in the resonance region. Our starting point is the DCC model that we have developed through a comprehensive analysis of $\pi N, \gamma p \rightarrow \pi N, \eta N, K\Lambda, K\Sigma$ data for $W \leq 2.1$ GeV [3]. In order to extend the DCC model of Ref. [3] to what works for the neutrino reactions, we analyzed data for the single pion photoproduction off the neutron, and also data for the electron scattering on both proton and neutron targets. Through the analysis, we determined the Q^2 -dependence of the vec-

tor form factors up to $Q^2 \leq 3 \text{ (GeV}/c)^2$. We derive the axial-current matrix elements that are linked to the πN potentials of the DCC model through the PCAC relation. As a consequence, relative phases between the non-resonant and resonant axial current amplitudes are uniquely determined within the DCC model.

We have presented cross sections for the neutrino-induced meson productions for $E_\nu \leq 2 \text{ GeV}$. In this energy region, the single-pion production gives the largest contribution. Towards $E_\nu \sim 2 \text{ GeV}$, the cross section for the double-pion production is getting larger to become 1/8 (1/4) of the single-pion production cross section for the proton (neutron) target. Because our DCC model has been determined by analyzing the $\pi N, \gamma N \rightarrow \pi N, \eta N, K\Lambda, K\Sigma$ data, we can also make a quantitative prediction for the neutrino cross sections for $\eta N, K\Lambda$, and $K\Sigma$ productions. We found that cross sections for $\eta N, K\Lambda$ and $K\Sigma$ productions are 10^{-2} - 10^{-3} times smaller than those for the single pion production. We have compared our numerical results with the available experimental data. For the single-pion production, our result, for which the axial N - N^* couplings are fixed by the PCAC relation, is consistent with the BNL data for $\nu_\mu p \rightarrow \mu^- \pi^+ p$, while fair agreement with both ANL and BNL data is found for the neutron target data. Through the comparison with the single pion production data for $W \lesssim 1.4 \text{ GeV}$ for which the $\Delta(1232)$ -excitation is the dominant mechanism, we were able to study the strength and the Q^2 -dependence of the axial N - $\Delta(1232)$ coupling. We also calculated double-pion production cross sections by taking account of relevant resonance contributions for the first time, and compared them with the data. We found a good agreement for $\nu_\mu p \rightarrow \mu^- \pi^+ \pi^0 p$ and $\nu_\mu n \rightarrow \mu^- \pi^+ \pi^- p$, but not for $\nu_\mu p \rightarrow \mu^- \pi^+ \pi^+ n$. Because the data for the double-pion productions are statistically rather poor, it is difficult to make a conclusive judgement on the DCC model.

Acknowledgments

The author thanks Hiroyuki Kamano and Toru Sato for their collaboration. This work was supported by Ministry of Education, Culture, Sports, Science and Technology (MEXT) KAKENHI Grant Number 25105010.

References

- [1] http://nuint.kek.jp/index_e.html; <http://j-parc-th.kek.jp/html/English/e-index.html>.
- [2] S.X. Nakamura, Y. Hayato, M. Hirai, H. Kamano, S. Kumano, M. Sakuda, K. Saito, and T. Sato: AIP Conf. Proc. **1663** (2015) 120010
- [3] H. Kamano, S. X. Nakamura, T.-S. H. Lee, and T. Sato: Phys. Rev. C **88** (2013) 035209
- [4] H. Kamano: Phys. Rev. C **88** (2013) 045203
- [5] H. Kamano, S. X. Nakamura, T.-S. H. Lee, and T. Sato: Phys. Rev. D **86** (2012) 097503
- [6] S. X. Nakamura, H. Kamano, T.-S. H. Lee, and T. Sato: arXiv:1506.03403.
- [7] V. Bernard et al.: J. Phys. **G28** (2002) R1
- [8] M.E. Christy and P. E. Bosted: Phys. Rev. C **81** (2010) 055213
- [9] H. Egiyan et al. (CLAS Collaboration): Phys. Rev. C **73** (2006) 025204
- [10] Preliminary results from JLab E00-002, C. Keppel, M.I. Niculescu, spokespersons. Data files can be obtained at <https://hallcweb.jlab.org/resdata/database>.
- [11] P.E. Bosted and M.E. Christy: Phys. Rev. C **77** (2008) 065206
- [12] M.E. Christy, private communication.
- [13] S. J. Barish et al.: Phys. Rev. D **19** (1979) 2521
- [14] T. Kitagaki et al.: Phys. Rev. D **34** (1986) 2554
- [15] C. Wilkinson, P. Rodrigues, S. Cartwright, L. Thompson, and K. McFarland: Phys. Rev. D **90** (2014) 112017
- [16] J.-J. Wu, T. Sato, and T.-S. H. Lee: Phys. Rev. C **91** (2015) 035203
- [17] T. Sato, D. Uno, and T.-S. H. Lee: Phys. Rev. C **67** (2003) 065201
- [18] S. N. Biswas, S. R. Choudhury, A. K. Goyal and J. N. Passi: Phys. Rev. D **18** (1978) 3187
- [19] S. A. Adjei, D. A. Dicus, and V. L. Teplitz: Phys. Rev. D **24** (1981) 623
- [20] E. Hernandez, J. Nieves, S.K. Singh, M. Valverde, and M.J. Vicente Vacas: Phys. Rev. D **77** (2008) 053009
- [21] D. Day et al.: Phys. Rev. D **28** (1983) 2714